

See discussions, stats, and author profiles for this publication at: <https://www.researchgate.net/publication/328078363>

# A Noise Compensation Mechanism for an RGNG-Based Grid Cell Model

Chapter in *Studies in Computational Intelligence* · January 2019

DOI: 10.1007/978-3-319-99283-9\_13

---

CITATION

1

READS

86

2 authors:



Jochen Kerdels

FernUniversität in Hagen

36 PUBLICATIONS 131 CITATIONS

[SEE PROFILE](#)



Gabriele Peters

FernUniversität in Hagen

88 PUBLICATIONS 565 CITATIONS

[SEE PROFILE](#)

Some of the authors of this publication are also working on these related projects:



CManipulator [View project](#)

# A Noise Compensation Mechanism for an RGNG-based Grid Cell Model

Jochen Kerdels and Gabriele Peters

University of Hagen, Universitätsstrasse 1 , D-58097 Hagen, Germany

**Abstract.** Grid cells of the entorhinal cortex provide a rare view on the deep stages of information processing in the mammalian brain. Complementary to earlier grid cell models that interpret the behavior of grid cells as specialized parts within a system for navigation and orientation we developed a grid cell model that facilitates an abstract computational perspective on the behavior of these cells. Recently, we investigated the ability of our model to cope with increasing levels of input signal noise as it would be expected to occur in natural neurobiological circuits. Here we investigate these results further and introduce a new noise compensation mechanism to our model that normalizes the output activity of simulated grid cells irrespective of whether or not input noise is present. We present results from an extended series of simulation runs to characterize the involved parameters.

## 1 Introduction

The parahippocampal-hippocampal region takes part in the deep stages of information processing in the mammalian brain. It is generally assumed to play a vital role in the formation of declarative, in particular episodic, memory as well as navigation and orientation. The discovery of *grid cells*, whose activity correlates with the animal's location in a regular pattern, facilitates a rare view on the neuronal processing that occurs in this region of the brain [7, 9]. Complementary to earlier computational models of grid cells that interpret the behavior of grid cells as specialized parts within a system for navigation and orientation [18, 23, 8, 1, 5, 19] we introduced a new grid cell model that views the behavior of grid cells as just one instance of a general information processing scheme [11, 10]. The model relies on principles of self-organisation facilitated by the recursive growing neural gas (RGNG) algorithm. We could demonstrate [10, 12] that our model can not only describe the basic properties of grid cell activity but also recently observed phenomena like *grid rescaling* [3, 2] as well as grid-like activity in primates that correlates with eye movements [14] instead of environmental location.

In addition, we recently investigated the ability of our model to cope with increasing levels of noise in its input signal as it would be expected to occur in natural neurobiological circuits [13]. Even with noise levels up to 90% of the input signal amplitude the model was able to establish the expected activity patterns. However, with increasing levels of noise the average maximum activity

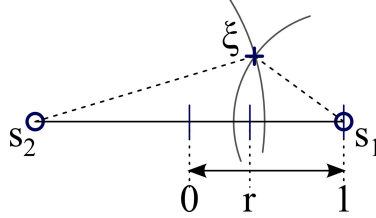


**Fig. 1.** Geometric interpretation of ratio  $r$ , which is used as a basis for an approximation of the modelled grid cell's activity. Extracted from [13].

of the model's output dropped by two orders of magnitude. Here we investigate this aspect further and present a noise compensation mechanism that we integrated in our grid cell model to normalize the average maximum output activity irrespective of whether or not input noise is present. The following section provides a short summary of our RGNG-based grid cell model, and section 3 revisits our previous results [13] and analyzes the effects of input noise further. Subsequently, section 4 introduces our proposed noise compensation mechanism and section 5 presents the results obtained using this mechanism over various parameter ranges. Finally, section 6 draws conclusions and outlines future work.

## 2 RGNG-based Grid Cell Model

The RGNG-based grid cell model is a neuron-centric model in which neurons act in their “own interest” while being in competition with each other. A biological neuron receives thousands of inputs from other neurons and the entirety of these inputs and their possible values constitute the neuron’s input space. We hypothesize that grid cells form a simple representation of their input space by learning a limited number of input patterns or *prototypes* that reflect the input space structure. Simultaneously, the competition among neurons in a local group of grid cells ensures that the simple representations learned by the individual cells are pairwise distinct and interleave in such a way that a complex representation of the input space emerges that is distributed over the entire group of neurons. We model this behavior by a two layer recursive growing neural gas that describes both the learning of prototypes within individual cells as well as the simultaneous competition among the cells in the group. Both processes are based on the same principles of self-organization utilizing a form of competitive Hebbian learning. For a formal description and an in-depth characterization of the model we refer to previous work [13, 10].

Here we focus on the operation of individual grid cells in the model. Their behavior is equivalent to that of a regular growing neural gas (GNG) as it was introduced by Fritzke [6]. A GNG is a network of units that is able to learn the topology of its input space. Each unit is associated with a *reference vector* or *prototype* that represents a local region of the input space. The neighborhood

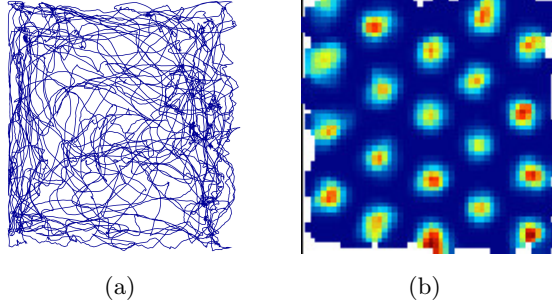


**Fig. 2.** (a) Example trace of rat movement within a rectangular,  $1\text{ m} \times 1\text{ m}$  environment recorded for a duration of 10 minutes. Movement data published by Sargolini et al. [21]. (b) Color-coded firing rate map of a simulated grid cell ranging from dark blue (no activity) to red (maximum activity). Extracted from [13].

relations of these local regions are reflected by the GNG network topology. In contrast to the original notion of GNG units as individual neurons our model interprets the GNG units as different dendritic subsections of a *single* grid cell. Thus, we assume that competitive Hebbian learning can occur within the dendritic tree of a single neuron allowing the neuron to respond to multiple, different input patterns and to facilitate the formation of a simple prototype-based representation of the neuron's input space.

The basic learning mechanism selects for every input  $\xi$  the best and second best matching units (BMUs)  $s_1$  and  $s_2$  whose prototypes  $s_1.w$  and  $s_2.w$  are closest to the input  $\xi$  according to a distance function  $D$ . The GNG network is then updated by creating (or refreshing) an edge between  $s_1$  and  $s_2$  and the prototype of the BMU  $s_1$  as well as the prototypes of all units connected to  $s_1$  are adapted towards the input  $\xi$ . In addition, the output activity  $a_u$  of the modelled grid cell  $u$  in response to the input  $\xi$  is determined based on the relative distances of  $\xi$  towards  $s_1.w$  and  $s_2.w$ :

$$a_u := e^{-\frac{(1-r)^2}{2\sigma^2}},$$

with  $\sigma = 0.2$  and ratio  $r$ :

$$r := \frac{D(s_2.w, \xi) - D(s_1.w, \xi)}{D(s_1.w, s_2.w)},$$

using a distance function  $D$ . Figure 1 provides a geometric interpretation of the ratio  $r$ . If input  $\xi$  is close to BMU  $s_1$  in relation to  $s_2$ , ratio  $r$  becomes 1. If on the other hand input  $\xi$  has about the same distance to  $s_1$  as it has to  $s_2$ , ratio  $r$  becomes 0.

Based on this measure of activity it becomes possible to correlate the simulated grid cell's activity with further variables, e.g., the recorded location of an

animal (Fig. 2a) in a typical experimental setup to study grid cells. Figure 2b shows such a correlation as a *firing rate map*, which is constructed according to the procedures described by Sargolini et al. [21] but using a  $5 \times 5$  boxcar filter for smoothing instead of a Gaussian kernel as introduced by Stensola et al. [22]. This conforms to the de facto standard of rate map construction in the grid cell literature. Each rate map integrates position and activity data over 30000 time steps corresponding to a single experimental trial with a duration of 10 minutes recorded at 50Hz.

### 3 Noise Resilience Revisited

Typical neurons in the the parahippocampal-hippocampal region of the brain have peak firing rates that range between 1Hz and 50Hz [9, 21, 4, 16]. Some proportion of this firing rate is due to spontaneous activity of the corresponding neuron. According to Koch [15] this random activity can occur about once per second, i.e., at 1Hz. Hence, the proportion of noise in a normalized firing rate resulting from this spontaneous firing can be expected to lie between 1.0 and 0.02 given the peak firing rates stated above.

We recently investigated the ability of the RGNG-based grid cell model to cope with noise in it's input signal that is caused by this spontaneous neural activity [13]. Since the model uses a vector of normalized neuronal activity as it's input signal, the proportion of noise in each input dimension depends on the assumed peak firing rate of the corresponding input neuron. Unfortunately, there is no empirical data on the distribution of peak firing rates in the input signal of biological grid cells. Thus, we assumed a uniform distribution and tested the model with increasing levels  $\xi_n$  of noise reflecting assumed minimal peak firing rates. For example, a maximum noise level of  $\xi_n = 0.1$  corresponds to a minimal peak firing rate of 10Hz, and a level of  $\xi_n = 0.5$  corresponds to a minimal peak firing rate of 2Hz in the input neurons.

The input signal used in the experiments was constructed by assuming that the animal location is encoded by two ensembles of input neurons that operate as one-dimensional ring attractor networks. In these networks a stable “bump” of activity encodes a linear position in a given direction. If the animal moves in that direction, the bump of activity is moved accordingly updating the encoded position. Similar types of input signals for grid cell models were proposed in the literature by, e.g., Mhatre et al. [17] as well as Pilly and Grossberg [20]. Formally, the input signal  $\xi := (v^x, v^y)$  was implemented as two concatenated 50-dimensional vectors  $v^x$  and  $v^y$ . To generate an input signal a position  $(x, y) \in [0, 1] \times [0, 1]$  was read from traces (Fig. 2a) of recorded rat movements that were published by Sargolini et al. [21] and mapped onto the corresponding elements of  $v^x$  and  $v^y$  as follows:

$$v_i^x := \max \left( 1 - \left| \frac{i - \lfloor dx + 0.5 \rfloor}{s} \right|, 1 - \left| \frac{d+i - \lfloor dx + 0.5 \rfloor}{s} \right|, 0 \right),$$

$$v_i^y := \max \left( 1 - \left| \frac{i - \lfloor dy + 0.5 \rfloor}{s} \right|, 1 - \left| \frac{d+i - \lfloor dy + 0.5 \rfloor}{s} \right|, 0 \right),$$

$$\forall i \in \{0 \dots d-1\},$$

with  $d = 50$  and  $s = 8$ . The parameter  $s$  controls the slope of the activity bump with higher values of  $s$  resulting in a broader bump. Each input vector  $\xi := (\tilde{v}^x, \tilde{v}^y)$  was then augmented by noise as follows:

$$\tilde{v}_i^x := \max[ \min[ v_i^x + \xi_n (2 U_{\text{rnd}} - 1), 1], 0],$$

$$\tilde{v}_i^y := \max[ \min[ v_i^y + \xi_n (2 U_{\text{rnd}} - 1), 1], 0],$$

$$\forall i \in \{0 \dots d-1\},$$

with maximum noise level  $\xi_n$  and uniform random values  $U_{\text{rnd}} \in [0, 1]$ .

Using this type of input we ran a series of simulation runs with increasing levels  $\xi_n$  of noise. Each run simulated a group of 100 grid cells with 20 dendritic subsections per cell using a fixed set of model parameters<sup>1</sup>. Figure 3 summarizes the results of these simulations. Each column corresponds to a single simulation run and shows an exemplary rate map of a grid cell chosen randomly from the 100 simulated cells (top row), the average maximum activity (MX) and the average minimum activity (MN) present in the rate maps of all simulated grid cells (below the rate map), the distribution of *gridness* scores<sup>2</sup> (middle row), and an activity function plot that indicates which values of ratio  $r$  corresponds to the respective average maximum activity (bottom row). The exemplary rate maps as well as the gridness score distributions show that the RGNG-based grid cell model is able to sustain the expected grid-like activity patterns despite increasing levels of noise in its input signal reflecting the robustness of the underlying principle of self-organisation. However, with increasing levels of noise the average maximum output activity of the simulated grid cells drops by two orders of magnitude,

---

<sup>1</sup> For a detailed description and motivation of all parameters we refer to [13].

<sup>2</sup> The *gridness score* ( $[-2, 2]$ ) is a measure of how grid-like the firing pattern of a neuron is. Neurons with gridness scores greater than 0.4 are commonly identified as grid cell.

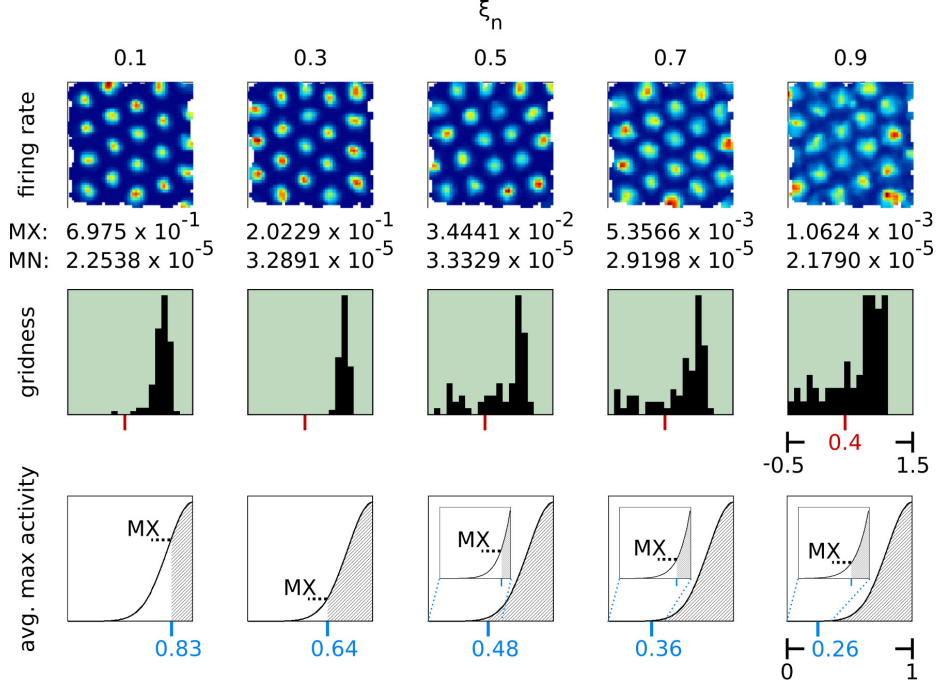


**Fig. 3.** Artificial rate maps (top row), gridness distributions (middle row), and activity function plots (bottom row) of simulation runs with varying levels  $\xi_n$  of noise (columns) added to the inputs. All simulation runs used a fixed set of parameters [13] and processed location inputs derived from movement data published by Sargolini et al. [21]. Each artificial rate map was chosen randomly from the particular set of rate maps. Average maximum activity (MX) and average minimum activity (MN) across all rate maps of a particular simulation given above gridness distributions. Gridness threshold of 0.4 indicated by red marks. Values of ratio  $r$  at average maximum activity (MX) given in blue. Insets show magnified regions of the activity function where MX values are low. Extracted from [13].

though the difference between average maximum and average minimum output activity is still at least two orders of magnitude for any tested noise level  $\xi_n$ .

The output activity  $a_u$  of a simulated grid cell  $u$  depends directly on the ratio  $r$ , which characterizes the relative distances between an input  $\xi$  and the prototypes of the best and second best matching units  $s_1$  and  $s_2$ . Only if the input  $\xi$  is much closer to the prototype  $s_1.w$  than  $s_2.w$ , the activity will approach a value of 1. Otherwise, if the distances between  $\xi$  and  $s_1.w$  as well as  $\xi$  and  $s_2.w$  are rather similar, the activity will be close to 0. This approximation of grid cell activity assumes that the input signals to the model originate from a sufficiently low-dimensional manifold in the high-dimensional input space. Only if this condition is met it is likely that some of the inputs will match the par-

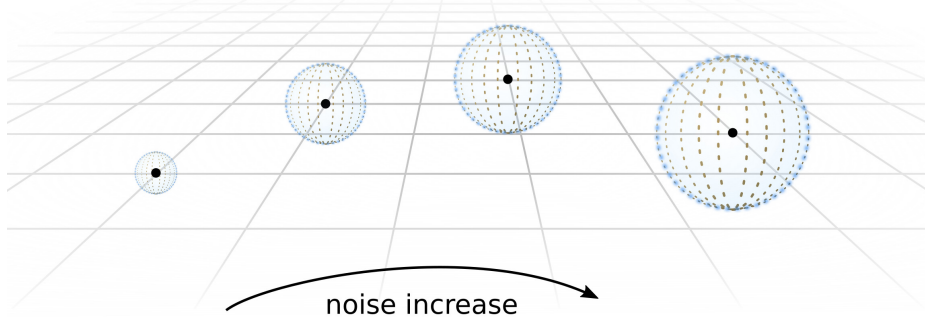


**Fig. 4.** Illustration of high-dimensional “dead zones” (blue-dotted spheres) surrounding prototypes (black dots) that lie on a lower-dimensional manifold. The “dead zones” grow with increasing levels of noise.

ticular best matching prototype closely resulting in a strong activation of the corresponding grid cell. Adding noise to inputs from such a lower-dimensional manifold moves the inputs away from the manifold in random directions. As a consequence, each of the grid cell’s prototypes becomes surrounded with a kind of “dead zone” for which it is unlikely that any input will originate from it (Fig. 4). This rather unintuitive property of randomness in high-dimensional space becomes more tangible if one considers the distribution of random points that lie within the unit sphere. For a point to lie close to the center of this sphere all of its coordinates must be close to zero. If the absolute value of only one coordinate is large, i.e., close to one or negative one, the point will lie close to the surface of the sphere. Thus, with increasing dimension it becomes more and more unlikely for a random point that the absolute values of all of its coordinates will be low. Likewise, it is equally unlikely that the high-dimensional noise added to an input will not move the input away from its low dimensional manifold, and hence move it away from the grid cell’s prototypes.

#### 4 Noise Compensation

The results summarized above suggest that real grid cells should be able to process inputs with low peak firing rates, that they may show a similar reduction in activity when the proportion of noise in their inputs is high, and that they should not suffer a degradation of their firing field geometry in the presence of noise. To the best of our knowledge no experiments were conducted yet that investigated the behavior of grid cells in response to (controlled) noise in their input signals. Since grid cells do show a wide range of peak firing rates [9, 21, 4, 16], possible variations of noise in their input signals may provide an explanation for these observations.

However, grid cells may also employ strategies to directly compensate for noise, e.g., by changing electrotonic properties of their cell membranes [15]. To account for this possibility we added a noise compensation mechanism to our model that normalizes ratio  $r$  with respect to the level of noise. Like the RGNG-based grid cell model itself the implemented noise compensation is a computational mechanism that is an abstract representation of this potential ability of grid cells and does not relate to any specific neurobiological implementation. As described above, the addition of noise to the inputs of the model results in “dead zones” around the prototypes of each grid cell that effectively limit the maximum value of ratio  $r$ . To normalize  $r$  without apriori knowledge about the level of noise that is present, it is necessary to identify and track the border region of these “dead zones” around each prototype. For that purpose a buffer  $b_N$  of size  $N$  was added to each unit  $s$  of a grid cell’s GNG containing the  $N$  largest values of ratio  $r$  encountered so far while  $s$  was the BMU. In addition, every entry of a buffer  $b_N$  has an *age* associated with it that is increased every time the simulated grid cell processes an input and the corresponding unit  $s$  is selected as BMU. Once the age of a buffer entry reaches a given age threshold  $A_{\max}$ , the value is evicted from the buffer. This way, changes in the level of input noise that influence the size of the “dead zones” can be tracked. Using this additional information a normalized ratio  $\hat{r}$  can then be defined as:

$$\hat{r} := \max \left[ \min \left[ \frac{r}{\widetilde{b}_N}, 1 \right], 0 \right],$$

with  $\widetilde{b}_N$  the median of all populated entries in buffer  $b_N$ .

## 5 Results

We characterized the normalized ratio  $\hat{r}$  by conducting a series of simulation runs that covered combinations of varying age thresholds  $A_{\max} \in \{50, 250, 750, 1500, 3000\}$ , varying buffer sizes  $N \in \{5, 11, 21, 41, 81\}$ , and varying levels of noise  $\xi_n \in \{0.1, 0.3, 0.7, 0.9\}$ . In addition, we reran corresponding simulations without normalizing ratio  $r$  to ensure that the input signal (including the random noise) was identical to the other simulations. All simulation runs used the same set of parameters as the previous simulations reported above and used the same location inputs derived from movement data published by Sargolini et al. [21]. However, the section of movement data that was analyzed here stems from a different experimental trial due to technical constraints of the simulation environment. This change resulted in slight variations in the gridness score distributions of the rerun results (compare figures 3 and 8).

Figures 5, 6, 7, and 8 summarize the simulation results of all simulation runs. Figure 5 shows one exemplary rate map for each simulation run. The rate maps were chosen randomly from one of the 100 grid cells per simulation. Figure 6 shows corresponding activity histograms that show the distribution of activity

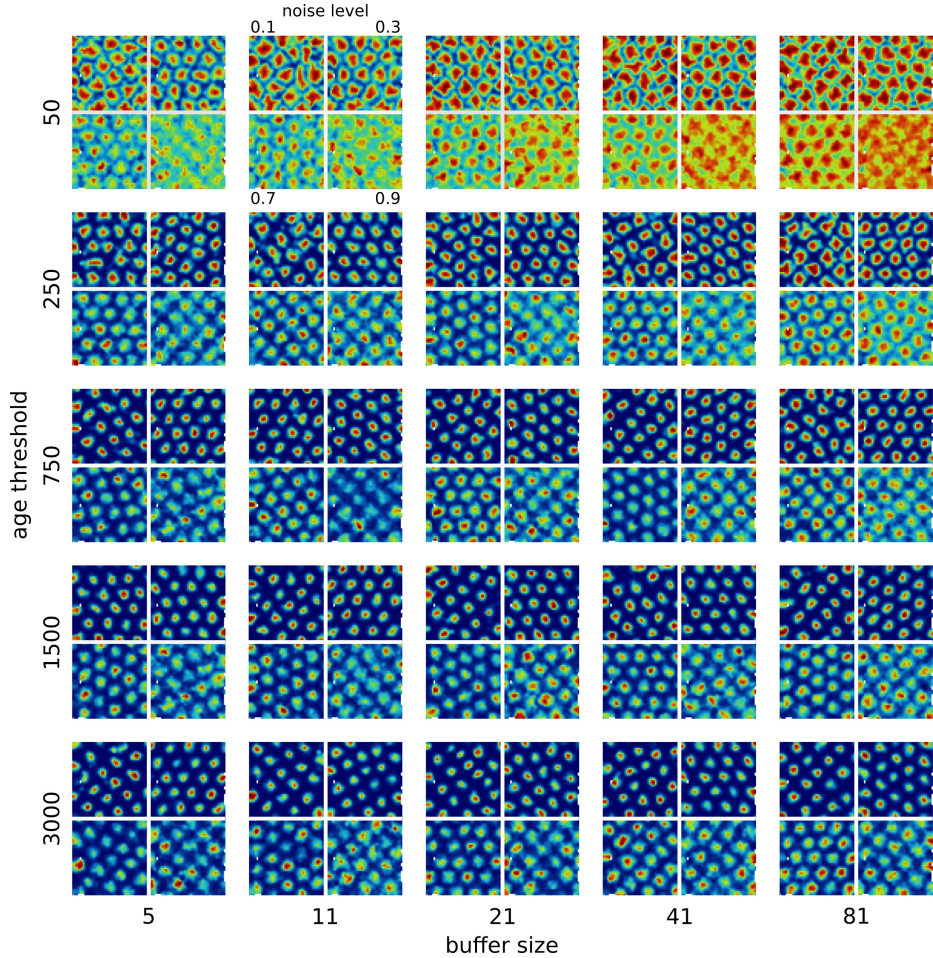


**Fig. 5.** Randomly chosen exemplary rate maps of simulation runs with varying age thresholds  $A_{\max} \in \{50, 250, 750, 1500, 3000\}$  (rows), varying buffer sizes  $N \in \{5, 11, 21, 41, 81\}$  (columns), and varying levels of noise  $\xi_n \in \{0.1, 0.3, 0.7, 0.9\}$  (quadrants of  $2 \times 2$  blocks). All simulation runs used the same set of parameters as the simulation runs underlying the data presented in figure 3 and processed location inputs derived from movement data published by Sargolini et al. [21].

values present in all rate maps (100) within each simulation. Figure 7 provides for each simulation run a histogram of gridness scores calculated based on the corresponding firing rate maps. Lastly, figure 8 shows the results of the simulation reruns with non-normalized ratio  $r$  for comparison.

The firing rate maps shown in figure 5 reflect the influence of the two parameters  $A_{\max}$  and  $N$  on the normalized ratio  $\hat{r}$  in an intuitive way. The age threshold

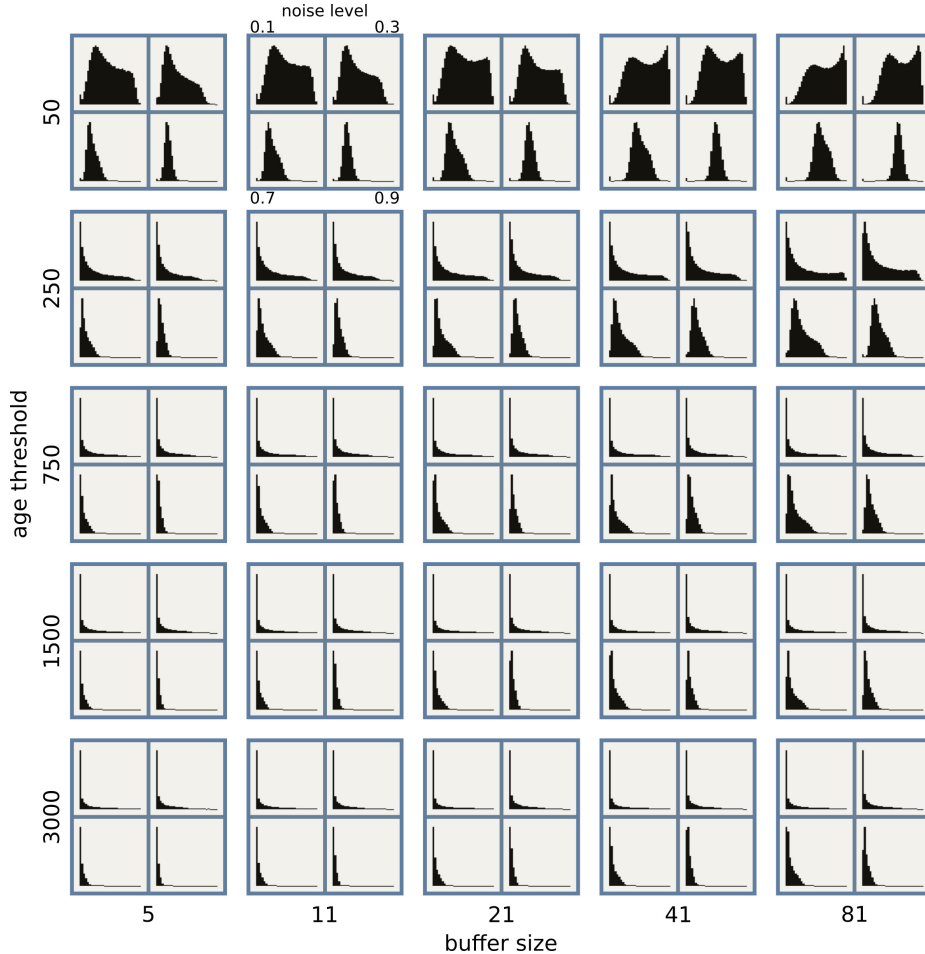


**Fig. 6.** Distributions of the activity values present in the firing rate maps of individual simulation runs. The shown data corresponds to the simulation runs shown in figure 5. The histograms range from 0 to 1.

$A_{\max}$  determines the duration for which a recently encountered large value of non-normalized ratio  $r$  is kept in the buffer and used to determine the “dead zone” boundary surrounding the corresponding prototype. With 20 dendritic subsections, i.e., prototypes per grid cell and 30000 time steps per 10 minute trial, each prototype will be BMU for about 1500 time steps per trial or 2.5 time steps per second *on average*. Thus, with an age threshold of  $A_{\max} = 50$  recently encountered large values of  $r$  are kept for about 20 seconds in the buffer before they are evicted. Larger values of  $A_{\max}$  prolong this time:

$$\begin{aligned}
A_{\max} = 50 &\rightarrow 20 \text{ sec} , \\
A_{\max} = 250 &\rightarrow 100 \text{ sec} , \\
A_{\max} = 750 &\rightarrow 300 \text{ sec (5 min)} , \\
A_{\max} = 1500 &\rightarrow 600 \text{ sec (10 min)} , \\
A_{\max} = 3000 &\rightarrow 1200 \text{ sec (20 min)} .
\end{aligned}$$

Similarly, the buffer size  $N$  does not only define how many values of non-normalized ratio  $r$  are used to estimate a “dead zone” boundary, but it also implies how much time is needed to fill the buffer on average:

$$\begin{aligned}
N = 5 &\rightarrow 2.0 \text{ sec}, \\
N = 11 &\rightarrow 4.4 \text{ sec}, \\
N = 21 &\rightarrow 8.4 \text{ sec}, \\
N = 41 &\rightarrow 16.4 \text{ sec}, \\
N = 81 &\rightarrow 32.4 \text{ sec}.
\end{aligned}$$

In cases where the age threshold  $A_{\max}$  is small and the buffer size  $N$  is large, the encountered values of ratio  $r$  are evicted faster than the buffer can be filled. As a consequence effectively all recent values of  $r$  are used to estimate the respective “dead zone” boundary. This effect can be observed in the first row of figure 5. With increasing buffer size the estimated “dead zone” boundary of each prototype moves towards the median of all encountered values of ratio  $r$  resulting in enlarged firing fields that are separated by only thin regions of lower activity. This overestimation of “dead zone” sizes is also reflected by the corresponding activity distributions shown in the first row of figure 6. The distributions are either unimodal or bimodal instead of being long-tail distributions as one would expect in case of a typical grid cell firing pattern (compare Fig. 8, middle). Especially in cases of high levels of noise ( $\xi_n \geq 0.7$ ) and larger buffer sizes ( $N \geq 21$ ) the minimum activity of the simulated cells increases to levels where the cell exhibits an unnatural continuous base level activity regardless of its particular input.

With increasing age threshold  $A_{\max}$  the time window in which the buffer can be filled with values of ratio  $r$  that are actually among the highest values that are likely to occur given the particular noise level increases. Consequently, the quality of the estimation of the particular “dead zone” boundary increases as well, which is reflected by decreasing sizes of firing fields (Fig. 5) and more long-tail distributions of activity values (Fig. 6). The activity distributions reveal that independent of a particular combination of age threshold and buffer size the tails of the distributions decrease with increasing levels of noise. Thus, the maximum activity of a simulated cell with normalized ratio  $\hat{r}$  still decreases with noise, but the magnitude of this decrease is significantly lower compared to the decrease when the activity is based on a non-normalized ratio  $r$  (figures 3 and 8). In fact, the decrease in maximum activity due to noise using the normalized ratio  $\hat{r}$  now matches the observed variability of peak firing rates in biological grid cells.

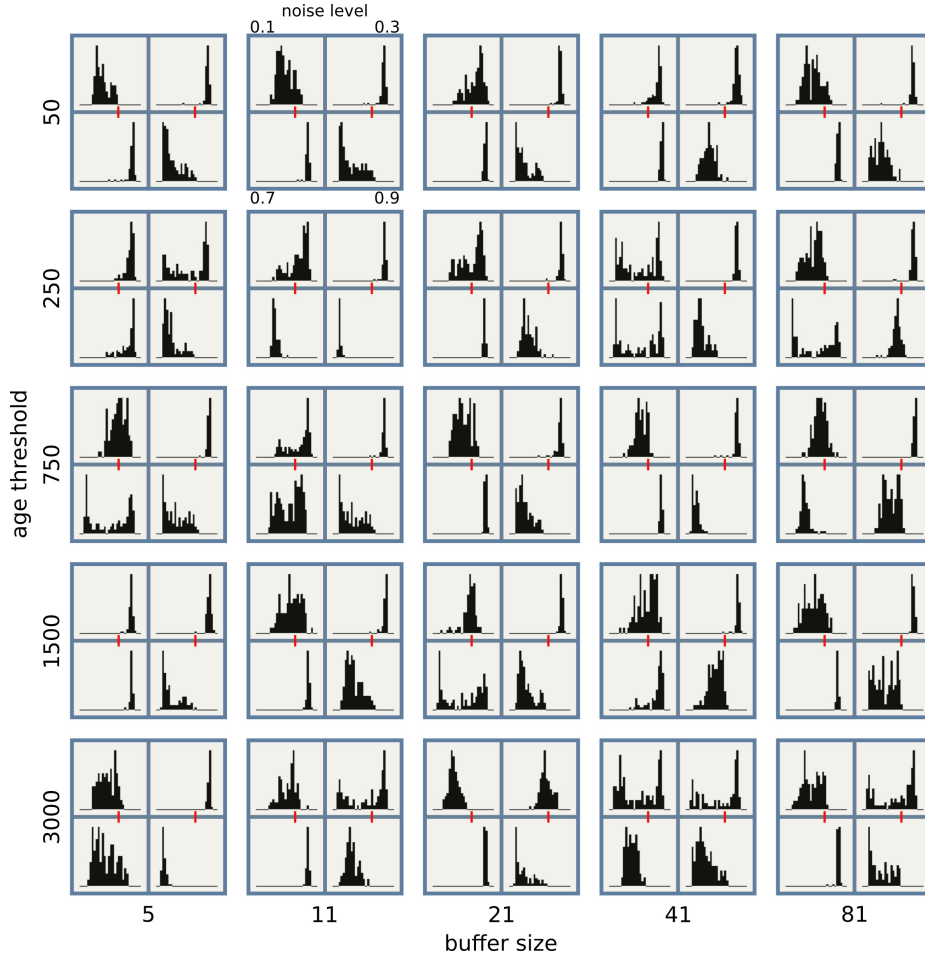


**Fig. 7.** Distributions of gridness scores calculated from the firing rate maps of individual simulation runs. The shown data corresponds to the simulation runs shown in figure 5. The histograms range from  $-1.5$  to  $+1.5$ . Gridness score threshold of  $0.4$  indicated by red mark.

The influence of normalizing ratio  $r$  on the resulting gridness scores of the simulated grid cells is inconclusive (Fig. 7). In general, there appears to be a pattern where the gridness scores increase with low to medium levels of noise before they decrease again when the levels of noise increase further. Small amounts of noise may prevent the learning algorithm from getting stuck in local minima and thus may result in hexagonal firing patterns that are more regular. However, some simulation runs (e.g.,  $A_{\max} = 750, N = 5$ ) deviate from this pattern and exhibit rather broad distributions of gridness score values at a noise level

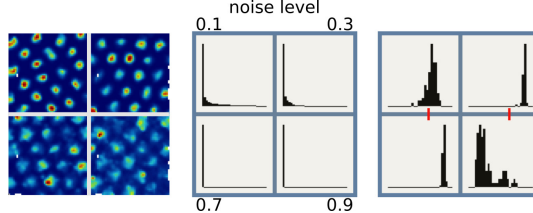


**Fig. 8.** Randomly chosen exemplary rate maps (left), distributions of activity values (middle), and distributions of gridness scores (right) from simulation runs with varying levels of noise  $\xi_n \in \{0.1, 0.3, 0.7, 0.9\}$  (quadrants of  $2 \times 2$  blocks) using **no noise compensation**. All other parameters were identical to the simulation runs presented in figures 5, 6, and 7.

of  $\xi_n = 0.7$ , but a clear correlation with the parameters age threshold or buffer size is not recognizable. One likely explanation for the observed variability in gridness score distributions is the alignment of grid cell firing patterns in the RGNG-based grid cell model. In common with biological grid cells, a group of grid cells modeled by the RGNG-based model align the rotation and spacing of their firing patterns in a self-organizing manner. Depending on initial conditions and the input presented so far this alignment process can get stuck in a stable configuration that introduces irregularities in the otherwise hexagonal firing patterns of the simulated grid cells (e.g.,  $A_{\max} = 1500, N = 41, \xi_n = 0.1$  in figure 5). As similar “defects” in the firing patterns of biological grid cells were experimentally observed and documented by Krupic et al. [16], it is inconclusive if this property of the RGNG-based model is a “bug” or a “feature”. In the grid cell literature it is rather common to exclude the firing rate maps of cells with gridness scores lower than a given threshold (around 0.3 to 0.4) from publication resulting in a lack of knowledge about cells that are *almost* grid cells given their firing rate maps.

## 6 Conclusions

We presented a noise compensation mechanism for our RGNG-based grid cell model based on a dynamic normalization of the core measure used to derive the activity of a simulated grid cell. The normalization is controlled by two parameters, age threshold  $A_{\max}$  and buffer size  $N$ , whose influence we characterized by an extended series of simulation runs. The results indicate that the age threshold parameter is more critical than the buffer size parameter. It should have a value that translates to a sliding time window of at least 5 minutes (in the context of the underlying experimental setup) in which unnormalized values are collected and used to dynamically estimate the normalization factor needed for the currently present noise level.

The proposed normalization procedure reduces the previously observed [13] drop in the output activity of simulated grid cells in the presence of high levels

of input noise by one order of magnitude. The remaining reduction in output activity matches the observed variability of peak firing rates in biological grid cells. If there is a possible connection between the peak firing rates of grid cells and the level of noise present in their input signal is an open question and remains to be investigated.

## References

1. Barry, C., Burgess, N.: Neural mechanisms of self-location. *Current Biology* 24(8), R330 – R339 (2014)
2. Barry, C., Ginzberg, L.L., OKeefe, J., Burgess, N.: Grid cell firing patterns signal environmental novelty by expansion. *Proceedings of the National Academy of Sciences* 109(43), 17687–17692 (2012)
3. Barry, C., Hayman, R., Burgess, N., Jeffery, K.J.: Experience-dependent rescaling of entorhinal grids. *Nat Neurosci* 10(6), 682–684 (jun 2007)
4. Boccanfuso, C.N., Sargolini, F., Thoresen, V.H., Solstad, T., Witter, M.P., Moser, E.I., Moser, M.B.: Grid cells in pre- and parasubiculum. *Nat Neurosci* 13(8), 987–994 (Aug 2010)
5. Burak, Y.: Spatial coding and attractor dynamics of grid cells in the entorhinal cortex. *Current Opinion in Neurobiology* 25(0), 169 – 175 (2014), theoretical and computational neuroscience
6. Fritzke, B.: A growing neural gas network learns topologies. In: *Advances in Neural Information Processing Systems* 7. pp. 625–632. MIT Press (1995)
7. Fyhn, M., Molden, S., Witter, M.P., Moser, E.I., Moser, M.B.: Spatial representation in the entorhinal cortex. *Science* 305(5688), 1258–1264 (2004)
8. Giocomo, L., Moser, M.B., Moser, E.: Computational models of grid cells. *Neuron* 71(4), 589 – 603 (2011)
9. Hafting, T., Fyhn, M., Molden, S., Moser, M.B., Moser, E.I.: Microstructure of a spatial map in the entorhinal cortex. *Nature* 436(7052), 801–806 (Aug 2005)
10. Kerdels, J.: A Computational Model of Grid Cells based on a Recursive Growing Neural Gas. Ph.D. thesis, FernUniversität in Hagen, Hagen (2016)
11. Kerdels, J., Peters, G.: A new view on grid cells beyond the cognitive map hypothesis. In: *8th Conference on Artificial General Intelligence (AGI 2015)* (July 2015)
12. Kerdels, J., Peters, G.: Modelling the grid-like encoding of visual space in primates. In: *Proceedings of the 8th International Joint Conference on Computational Intelligence, IJCCI 2016, Volume 3: NCTA, Porto, Portugal, November 9-11, 2016.* pp. 42–49 (2016)
13. Kerdels, J., Peters, G.: Noise resilience of an rgng-based grid cell model. In: *Proceedings of the 8th International Joint Conference on Computational Intelligence, IJCCI 2016, Volume 3: NCTA, Porto, Portugal, November 9-11, 2016.* pp. 33–41 (2016)
14. Killian, N.J., Jutras, M.J., Buffalo, E.A.: A map of visual space in the primate entorhinal cortex. *Nature* 491(7426), 761–764 (Nov 2012)
15. Koch, C.: *Biophysics of Computation: Information Processing in Single Neurons*. Computational Neuroscience Series, Oxford University Press, USA (2004), <http://books.google.de/books?id=J9juLkO7p80C>
16. Krupic, J., Burgess, N., OKeefe, J.: Neural representations of location composed of spatially periodic bands. *Science* 337(6096), 853–857 (2012)

17. Mhatre, H., Gorchetchnikov, A., Grossberg, S.: Grid cell hexagonal patterns formed by fast self-organized learning within entorhinal cortex (published online 2010). *Hippocampus* 22(2), 320–334 (2010)
18. Moser, E.I., Moser, M.B.: A metric for space. *Hippocampus* 18(12), 1142–1156 (2008)
19. Moser, E.I., Moser, M.B., Roudi, Y.: Network mechanisms of grid cells. *Philosophical Transactions of the Royal Society B: Biological Sciences* 369(1635) (2014)
20. Pilly, P.K., Grossberg, S.: How do spatial learning and memory occur in the brain? coordinated learning of entorhinal grid cells and hippocampal place cells. *J. Cognitive Neuroscience* pp. 1031–1054 (2012)
21. Sargolini, F., Fyhn, M., Hafting, T., McNaughton, B.L., Witter, M.P., Moser, M.B., Moser, E.I.: Conjunctive representation of position, direction, and velocity in entorhinal cortex. *Science* 312(5774), 758–762 (2006)
22. Stensola, H., Stensola, T., Solstad, T., Froland, K., Moser, M.B., Moser, E.I.: The entorhinal grid map is discretized. *Nature* 492(7427), 72–78 (Dec 2012)
23. Welinder, P.E., Burak, Y., Fiete, I.R.: Grid cells: The position code, neural network models of activity, and the problem of learning. *Hippocampus* 18(12), 1283–1300 (2008)